

# Multipole Models of Four-Image Gravitational Lenses with Anomalous Flux Ratios

Arthur B. Congdon and Charles R. Keeton

*Department of Physics and Astronomy, Rutgers University, 136 Frelinghuysen Road, Piscataway, NJ 08854 USA*

Accepted in MNRAS

## ABSTRACT

It has been known for over a decade that many four-image gravitational lenses exhibit anomalous radio flux ratios. These anomalies can be explained by adding a clumpy cold dark matter (CDM) component to the background galactic potential of the lens. As an alternative, Evans & Witt (2003) recently suggested that smooth multipole perturbations provide a reasonable alternative to CDM substructure in some but not all cases. We generalize their method in two ways so as to determine whether multipole models can explain highly anomalous systems. We carry the multipole expansion to higher order, and also include external tidal shear as a free parameter. Fitting for the shear proves crucial to finding a physical (positive-definite density) model. For B1422+231, working to order  $k_{\max} = 5$  (and including shear) yields a model that is physical but implausible. Going to higher order ( $k_{\max} \gtrsim 9$ ) reduces global departures from ellipticity, but at the cost of introducing small scale wiggles in proximity to the bright images. These localized undulations are more pronounced in B2045+265, where  $k_{\max} \sim 17$  multipoles are required to smooth out large scale deviations from elliptical symmetry. Such modes surely cannot be taken at face value; they must indicate that the models are trying to reproduce some other sort of structure. Our formalism naturally finds models that fit the data exactly, but we use B0712+472 to show that measurement uncertainties have little effect on our results. Finally, we consider the system B1933+503, where two sources are lensed by the same foreground galaxy. The additional constraints provided by the images of the second source render the multipole model unphysical. We conclude that external shear must be taken into account to obtain plausible models, and that a purely smooth angular structure for the lens galaxy does not provide a viable alternative to the prevailing CDM clump hypothesis.

**Key words:** galaxies: haloes — galaxies: structure — dark matter — gravitational lensing

## 1 INTRODUCTION

It has been suspected since the time of Newton that a light ray would be deflected when it passes near a massive object. This phenomenon, now known as gravitational lensing, provided one of the earliest and best tests of the validity of general relativity. Since that time, lens theory has matured into an active field of astronomy (see Kochanek et al. 2004, for a recent review). Probing the structure of galaxies is one of the many areas to which lensing has been applied over the past fifteen years (e.g., Kochanek 1991; Keeton et al. 1998). Because lensing is sensitive to all mass, it is possible to study both dark and luminous components within galaxies.

In the case of strong lensing where the light source is multiply imaged, we can use the positions and fluxes of the images to study small-scale structure within the lens

galaxy. This technique can be most readily applied to four-image systems in a cusp or fold configuration, which occurs when the angular separation between the lens and source is small. For a cusp lens we expect the three brightest images to satisfy the magnification sum rule (e.g., Schneider & Weiss 1992; Mao & Schneider 1998; Keeton et al. 2003),

$$\mu_1 + \mu_2 + \mu_3 \approx 0. \quad (1)$$

In the fold case an analogous relation holds for the two brightest images (Gaudi & Petters 2002; Keeton et al. 2005):

$$\mu_1 + \mu_2 \approx 0. \quad (2)$$

Although these relations should hold for all smooth lens potentials, there are a number of observed systems for which they are violated (Mao & Schneider 1998; Keeton et al. 2003, 2005). Since the magnifications are not directly observable,

we refer to systems that violate the sum rule as exhibiting flux ratio anomalies, with the observed fluxes being related to the magnifications by the flux of the source.

One might argue that violations of the magnification sum rule originate in electromagnetic effects of the interstellar medium on light emitted by the lensed source. However, dust extinction is negligible at radio wavelengths, which are much larger than the typical size of a dust grain. The lack of wavelength dependence in radio flux ratios rules out electromagnetic effects as an explanation for radio anomalies (see e.g., Kochanek & Dalal 2004; Keeton et al. 2003, 2005, and references therein).

Explaining the observed anomalies therefore requires the addition of small-scale structure to the gravitational potential of the galaxy (Mao & Schneider 1998). A possible candidate for this substructure emerged through the work of Moore et al. (1999) and Klypin et al. (1999), whose numerical simulations predicted a quantity of cold dark matter (CDM) halos with masses  $\sim 10^6 - 10^8 M_\odot$ , greatly exceeding the observed numbers of such objects. This result motivated Metcalf & Madau (2001) to consider how the abundance of predicted CDM substructure might affect lensing. They pointed out that even if the small halos are completely dark — invisible to standard luminosity-based studies — they could still affect lens flux ratios and perhaps explain the observed anomalies. Indeed, Dalal & Kochanek (2002) found that putting  $\sim 2\%$  of the mass in  $\sim 10^6 M_\odot$  halos could reproduce the observed flux ratios for seven anomalous lens systems, while broadly matching the predictions of the numerical simulations. But does this mean that the flux ratio problem is really solved, and that the “missing” CDM satellites have been found? Are there other plausible models that can solve the flux ratio problem?

Possibilities may include stellar microlensing, and complex structure such as isophote twists or triaxiality in the lens galaxy. Since the radio-emitting regions of the QSO sources we will consider have a much larger angular scale than the Einstein radius of a typical star in the lens galaxy, microlensing can be eliminated as a potential cause of flux ratio anomalies. That leaves the question of whether models that alter the global structure of the lens potential offer a viable explanation of flux ratio anomalies. Our goal is to see whether we can fit four anomalous radio lenses using models with general but reasonable angular structure.

We begin with the self-similar multipole model of Evans & Witt (2003). In this framework, the potential of the lens galaxy is described by a generalized isothermal model whose angular dependence is expressed as a Fourier series. The multipole coefficients are determined by fitting the observed image positions and flux ratios. The truncation order of the series is chosen so that the matrix of constraints is square. Evans & Witt (2003) found that such a model could explain some but not all observed lenses. In particular, for B1422+231 (the only radio anomaly they studied), they could find a physically acceptable model only by inflating the errorbars on the data, and even that model was highly non-elliptical and implausible.

In this paper we extend the multipole formalism to include external shear — tidal distortions from objects near the lens galaxy (e.g., Keeton et al. 1997) — and higher order multipole modes. Shear in particular will prove essential for obtaining sensible solutions. While this is not the most

general method, it is mathematically simple and may be a reasonable alternative to substructure in some lenses.

As a test case, we first apply our model to Q2237+0305, which is not anomalous at radio wavelengths. Then, we apply the model to B1422+231, B2045+265, B0712+472, and B1933+503, which are all highly anomalous. An exhaustive study of the known radio anomalies would also include B1555+375, but the position of the lens galaxy (a key ingredient in our formalism) is unknown.

## 2 METHODS

We begin by writing the convergence (dimensionless surface mass density),  $\kappa$ , and lens potential,  $\psi$ , for a galaxy with a flat rotation curve and arbitrary angular structure. This model is often referred to as a generalized isothermal model (Witt et al. 2000; Zhao & Pronk 2001; Evans & Witt 2001, 2003):

$$\kappa(r, \theta) = \frac{1}{2r} G(\theta); \quad \psi(r, \theta) = rF(\theta). \quad (3)$$

Noting that  $\nabla^2 \psi = 2\kappa$ , we find that  $F$  and  $G$  are related by

$$G(\theta) = F(\theta) + F''(\theta). \quad (4)$$

For a given source position,  $\mathbf{u} \equiv (u, v)$ , we can find the image positions,  $\mathbf{x} \equiv (r \cos \theta, r \sin \theta)$ , via the lens equation,

$$\mathbf{u} = \mathbf{x} - \nabla \psi(\mathbf{x}). \quad (5)$$

The inverse magnification of an image at  $\mathbf{x}$  is given by

$$\mu^{-1} = \det \left( \frac{\partial \mathbf{u}}{\partial \mathbf{x}} \right) = 1 - \frac{G(\theta)}{r}. \quad (6)$$

An important property of the lens potential is the critical curve, along which the magnification is formally infinite. The critical curve in the image plane maps to the caustic in the source plane, which marks the transition between 2-image and 4-image systems. We see from equation (6) that the critical curve is given by  $r_{\text{crit}}(\theta) = G(\theta)$ , which is equivalent to the isodensity contour with  $\kappa = 1/2$ .

### 2.1 Multipole Lens Model of Evans & Witt (2003)

Let us write the angular part of the potential,  $F$ , as a multipole (Fourier) expansion in  $\theta$ , i.e.

$$F(\theta) \equiv \frac{a_0}{2} + \sum_{k=1}^{k_{\text{max}}} (a_k \cos k\theta + b_k \sin k\theta), \quad (7)$$

for some appropriate  $k_{\text{max}}$ . The Fourier coefficient  $a_0$  is related to the Einstein radius by  $R_{\text{Ein}} \equiv a_0/2$ . We can find the unknown source position,  $\mathbf{u}$ , and the Fourier coefficients,  $a_k$  and  $b_k$ , by introducing observational constraints, viz. the image positions and flux ratios.

From equations (3) and (7), the lens equation (5) becomes

$$u = r_l \cos \theta_l - \frac{a_0}{2} \alpha_0(\theta_l) - \sum_{k=1}^{k_{\text{max}}} [a_k \alpha_k(\theta_l) + b_k \beta_k(\theta_l)] \quad (8)$$

$$v = r_l \sin \theta_l - \frac{a_0}{2} \hat{\alpha}_0(\theta_l) - \sum_{k=1}^{k_{\text{max}}} [a_k \hat{\alpha}_k(\theta_l) + b_k \hat{\beta}_k(\theta_l)] \quad (9)$$

where  $l = 1, 2, \dots, n$  is the image number. The functions  $\alpha_k$ ,  $\hat{\alpha}_k$ ,  $\beta_k$ , and  $\hat{\beta}_k$  are defined in Evans & Witt (2003), equations (13) and (14):

$$\alpha_k(\theta) = \cos \theta \cos k\theta + k \sin \theta \sin k\theta, \quad (10)$$

$$\hat{\alpha}_k(\theta) = \sin \theta \cos k\theta - k \cos \theta \sin k\theta, \quad (11)$$

$$\beta_k(\theta) = \cos \theta \sin k\theta - k \sin \theta \cos k\theta, \quad (12)$$

$$\hat{\beta}_k(\theta) = \sin \theta \sin k\theta + k \cos \theta \cos k\theta. \quad (13)$$

Another set of constraints comes from the flux ratios. Relative to image  $n$ , we have

$$f_{nl} = \frac{\mu_n}{\mu_l}. \quad (14)$$

We then use (4), (6) and (7) to obtain

$$(f_{nl} - 1)r_n r_l = \frac{a_0}{2}\gamma_0(\theta_l) + \sum_{k=1}^{k_{\max}} [a_k \gamma_k(\theta_l) + b_k \delta_k(\theta_l)], \quad (15)$$

where  $l = 1, 2, \dots, n-1$ . The functions  $\gamma_k$  and  $\delta_k$  are defined by Evans & Witt (2003), equation (18):

$$\gamma_k(\theta_l) = (1 - k^2)[f_{nl} r_l \cos k\theta_n - r_n \cos k\theta_l] \quad (16)$$

$$\delta_k(\theta_l) = (1 - k^2)[f_{nl} r_l \sin k\theta_n - r_n \sin k\theta_l]. \quad (17)$$

We can combine equations (8), (9) and (15) into a single matrix equation:

$$\mathbf{A} \cdot \boldsymbol{\chi} = \mathbf{b}, \quad (18)$$

where  $\boldsymbol{\chi}$  is the  $(2k_{\max} + 1)$ -dimensional vector of parameters for which we are solving;  $\boldsymbol{\chi} = (u, v, a_0, a_2, b_2, \dots, a_{k_{\max}}, b_{k_{\max}})$ . We drop  $a_1$  and  $b_1$ , which represent an unobservable translation of coordinates in the source plane. The  $(3n - 1)$ -dimensional vector  $\mathbf{b}$  contains the observed image positions and flux ratios;

$$\mathbf{b} = (x_1, \dots, x_n, y_1, \dots, y_n, (f_{n1} - 1)r_n r_1, \dots, (f_{n,n-1} - 1)r_n r_{n-1}), \quad (19)$$

where  $x_l = r_l \cos \theta_l$  and  $y_l = r_l \sin \theta_l$ . The  $(3n - 1) \times (2k_{\max} + 1)$  matrix,  $\mathbf{A}$ , is defined in equation (22) of Evans & Witt (2003):

$$\mathbf{A} = \begin{bmatrix} 1 & 0 & \alpha_{01} & \alpha_{21} & \beta_{21} & \dots \\ \vdots & \vdots & \vdots & \vdots & \vdots & \vdots \\ 1 & 0 & \alpha_{0n} & \alpha_{2n} & \beta_{2n} & \dots \\ 0 & 1 & \hat{\alpha}_{01} & \hat{\alpha}_{21} & \hat{\beta}_{21} & \dots \\ \vdots & \vdots & \vdots & \vdots & \vdots & \vdots \\ 0 & 1 & \hat{\alpha}_{0n} & \hat{\alpha}_{2n} & \hat{\beta}_{2n} & \dots \\ 0 & 0 & \gamma_{01} & \gamma_{21} & \delta_{21} & \dots \\ \vdots & \vdots & \vdots & \vdots & \vdots & \vdots \\ 0 & 0 & \gamma_{0,n-1} & \gamma_{2,n-1} & \delta_{2,n-1} & \dots \end{bmatrix}, \quad (20)$$

where  $\alpha_{kl} \equiv \alpha_k(\theta_l)$  etc. Evans & Witt (2003) choose  $k_{\max}$  such that  $\mathbf{A}$  is square. We then have  $k_{\max} = 5$  for a 4-image system ( $n = 4$ ). With this choice of  $k_{\max}$  we can simply multiply equation (18) by  $\mathbf{A}^{-1}$  to solve for  $\boldsymbol{\chi}$ , provided that  $\mathbf{A}$  is non-singular. To ensure numerical stability, however, Evans & Witt (2003) solve for  $\boldsymbol{\chi}$  using *singular value decomposition* (SVD).

## 2.2 The Minimum Wiggle Model

There are two main limitations of the method of Evans & Witt (2003). On a technical point, their requirement that  $\mathbf{A}$  be square prevents one from probing the contributions of higher-order multipoles. More significantly, the effects of external shear have not been included for several of the systems they analyze. We now set out to address these two concerns.

In the case of arbitrary  $k_{\max}$ , SVD produces a particular solution  $\boldsymbol{\chi}^{(0)}$  as well as a basis for the null space of  $\mathbf{A}$ :  $\{\boldsymbol{\nu}^{(i)}\}$ . We then have a family of solutions,

$$\boldsymbol{\chi} = \boldsymbol{\chi}^{(0)} + \sum_{i=1}^{N_p - N_c} c_i \boldsymbol{\nu}^{(i)}, \quad (21)$$

where  $N_p = (3n - 1) > N_c = (2k_{\max} + 1)$  are the numbers of parameters and constraints, respectively. We must now select appropriate coefficients  $c_i$  in order to construct the most plausible solution. Since the lens galaxies we are considering are elliptical, it seems reasonable to find the model with the smallest deviation from elliptical symmetry. In other words, we want to minimize the wiggles in the isodensity contours.

For a curve of constant  $\kappa$ , the deviation  $\delta r(\theta)$  from perfect elliptical symmetry is given by:

$$\begin{aligned} \delta r(\theta) &\equiv r(\theta) - r_0(\theta), \\ &= \frac{1}{2\kappa} \sum_{k=3}^{k_{\max}} (1 - k^2) (a_k \cos k\theta + b_k \sin k\theta), \end{aligned} \quad (22)$$

where

$$r_0(\theta) = \frac{1}{2\kappa} \left[ \frac{a_0}{2} - 3(a_2 \cos 2\theta + b_2 \sin 2\theta) \right]$$

is an isodensity curve for a perfectly elliptical galaxy. To quantify the wiggles, we average  $\delta r^2$  over  $\theta$ :

$$\delta r_{\text{rms}}^2 \equiv \langle \delta r^2 \rangle_{\theta} = \frac{1}{8\kappa^2} \sum_{k=3}^{k_{\max}} (1 - k^2)^2 (a_k^2 + b_k^2). \quad (23)$$

We are interested in the solution for which the root mean square wiggle is minimized.

If we consider higher order multipoles but ignore shear, we simply need to minimize the RMS wiggle with respect to the coefficients  $c_i$ . Since  $\langle \delta r^2 \rangle$  is quadratic in  $a_k$  and  $b_k$ , and hence also in  $c_i$ , this minimization is straightforward.

When shear is included, the task of minimizing  $\langle \delta r^2 \rangle$  becomes slightly more involved. In particular, the lens potential of equation (3) must be modified:

$$\psi(r, \theta) = rF(\theta) - \frac{\gamma_1}{2} r^2 \cos 2\theta - \frac{\gamma_2}{2} r^2 \sin 2\theta, \quad (24)$$

for constants  $\gamma_1, \gamma_2$ . This modification requires that the functions  $\gamma_k$  and  $\delta_k$  of equation (15), and the vector  $\mathbf{b}$  of equation (18) be redefined by the expressions of Appendix D of Evans & Witt (2003). Namely,

$$\gamma_k(\theta_l) = (1 - k^2) \left[ f_{nl} r_l \cos k\theta_n W(\theta_n) - r_n \cos k\theta_l W(\theta_l) \right] \quad (25)$$

$$\delta_k(\theta_l) = (1 - k^2) \left[ f_{nl} r_l \sin k\theta_n W(\theta_n) - r_n \sin k\theta_l W(\theta_l) \right] \quad (26)$$

where

$$W(\theta_l) = 1 + \gamma_1 \cos 2\theta_l + \gamma_2 \sin 2\theta_l \quad (27)$$

and

$$\mathbf{b} = \begin{aligned} & [(1 + \gamma_1)x_1 + \gamma_2 y_1, \dots, (1 + \gamma_1)x_n + \gamma_2 y_n, \\ & (1 - \gamma_1)y_1 + \gamma_2 x_1, \dots, (1 - \gamma_1)y_n + \gamma_2 x_n, \\ & (f_{n1} - 1)r_n r_1 (1 - \gamma_1^2 - \gamma_2^2), \dots, \\ & (f_{n,n-1} - 1)r_n r_{n-1} (1 - \gamma_1^2 - \gamma_2^2)]. \end{aligned} \quad (28)$$

We see that including  $(\gamma_1, \gamma_2)$  as parameters to be determined leads to a set of non-linear equations. To deal with this problem, we use a non-linear optimization procedure. For specific values of  $(\gamma_1, \gamma_2)$ , we can use SVD along with the minimum wiggle criterion to solve for the source position and Fourier coefficients. A minimization function can be employed to find the optimal values for  $(\gamma_1, \gamma_2)$ . We refer to the resulting solution as the *minimum wiggle model*.

### 3 RESULTS

Let us now apply our methods to five quadruply imaged quasars. We begin with the Einstein cross, Q2237+0305, which does not exhibit anomalous flux ratios at radio wavelengths, thus providing a simple test case for the multipole expansion approach. Figure 1 shows a model with  $k_{\max} = 5$  and no external shear (cf. Evans & Witt 2003, Figure 2). The model exactly fits the observational data presented by Falco et al. (1996) and the CASTLES website. The elliptical appearance of the isodensity contour confirms that the multipole method can find reasonable solutions in lens systems that do not require small-scale structure. Now let us turn to four anomalous systems: B1422+231, B2045+265, B0712+472, and B1933+503.

#### 3.1 External Shear

To motivate the need for external shear, we first study B1422+231 using a model that does not include shear. To facilitate comparison with the results of Evans & Witt (2003), we consider a fifth order multipole model, which fits the data of Impey et al. (1996) and Patnaik et al. (1999) exactly. It is clear from Figure 2(a) that this model is unphysical. In addition to having a completely nonelliptical appearance, the model isodensity contour crosses the origin indicating that  $r$  becomes negative. Evans & Witt (2003) found a slightly better solution by inflating the measurement uncertainties (see their Figure 6). Even so, the model is incompatible with the observed structure of elliptical galaxies, a point noted by the authors.

When we extend the model by including shear, it becomes possible to find a physical — albeit not necessarily plausible — angular structure for the lens galaxy (see Figure 2(b)). Before we can draw any conclusions from this result, however, we must determine whether the shear parameters and Fourier coefficients we obtain are compatible with other observations. The shear parameters we find for B1422+231 are reasonable, because the lens lies in a group of galaxies that create a strong tidal field (see Kundić et al. 1997; Momcheva et al. 2005). In particular, our shear amplitude of  $\gamma \equiv \sqrt{\gamma_1^2 + \gamma_2^2} = 0.172$ , and orientation

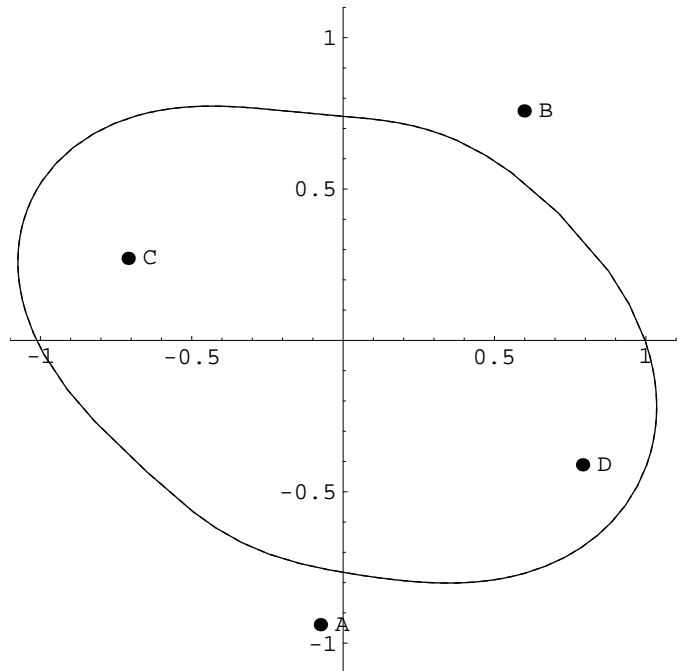


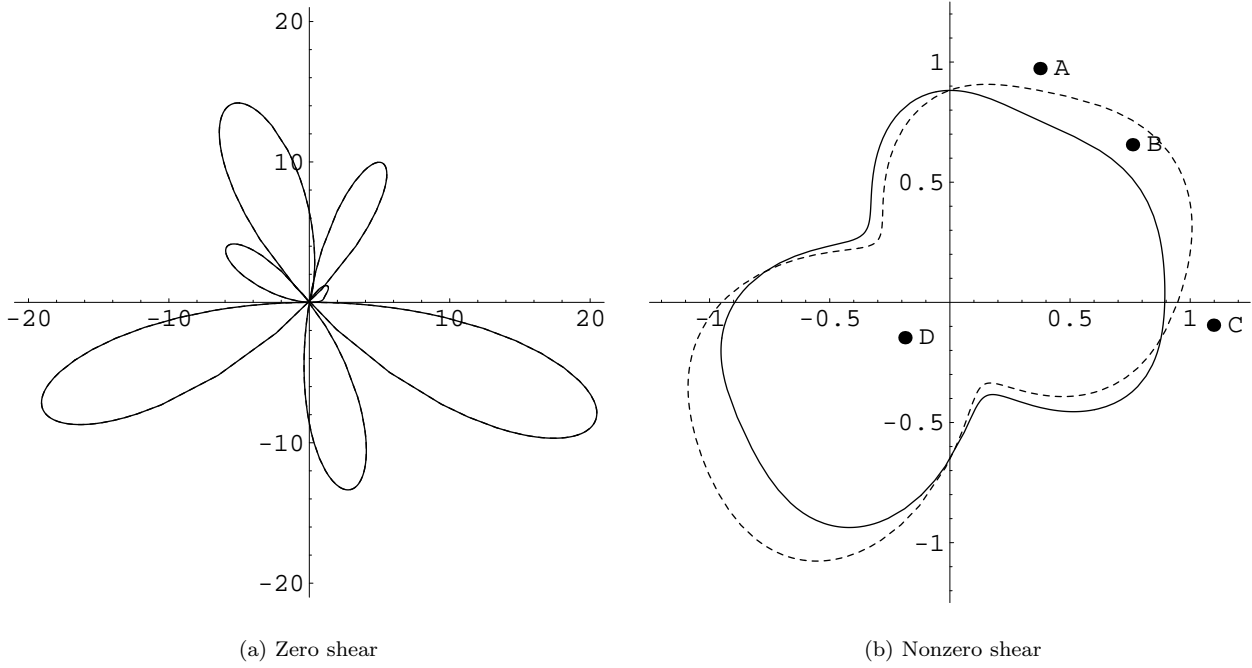
**Figure 1.** Isodensity contour with  $\kappa = 1/2$  (coincident with critical curve) for Q2237+0305 with  $k_{\max} = 5$  and no shear. The axes are labeled in arcseconds.

$\theta_\gamma \equiv (1/2) \tan^{-1}(\gamma_2/\gamma_1) = 40^\circ$  are similar to those quoted by Kundić et al. (1997).

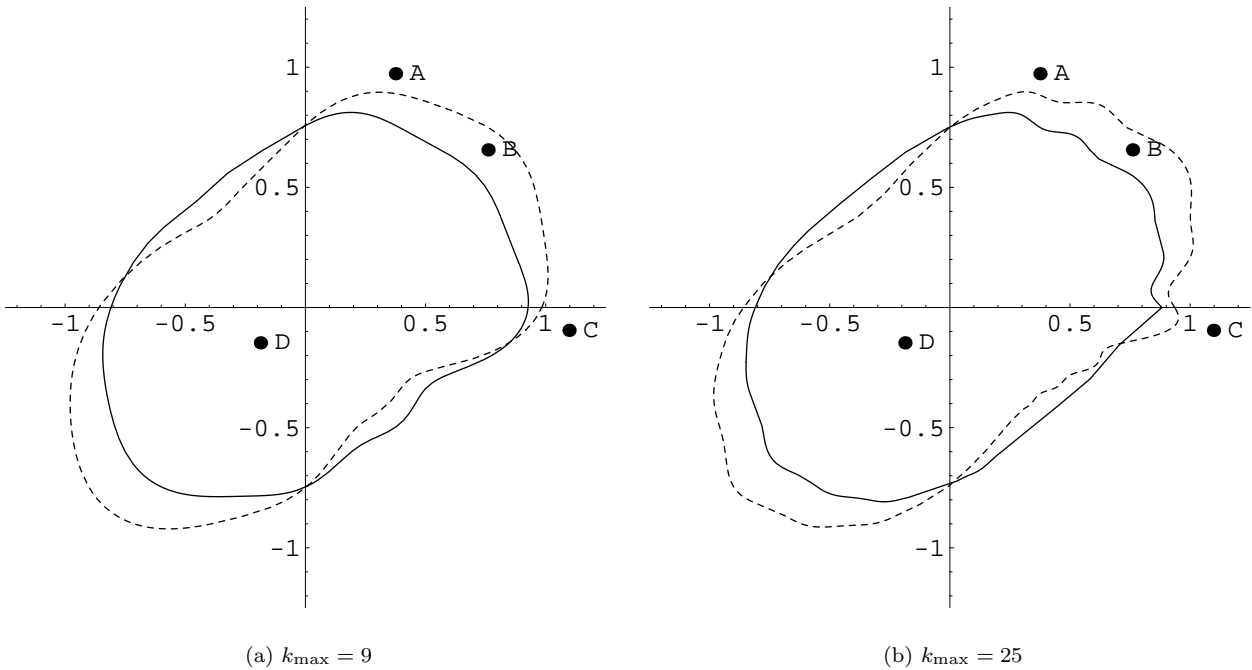
The Fourier coefficients through order 4, plus some other model properties, are given in Table 1. To interpret them, we can determine the dimensionless octopole amplitude,  $A_4$ , which describes the boxiness or diskiness of the isodensity contours, and compare it with the octopole amplitudes measured for the isophotes of elliptical galaxies. The comparison is not perfect because lens models involve the mass while observations involve the light, but we can at least get a sense of whether the lens models are reasonable. The octopole amplitude  $A_4$  is just the Fourier coefficient for the density, expressed in a coordinate frame aligned with the major axis of the galaxy, and normalized by the semi-major axis length. In terms of the coefficients in Table 1, the major axis lies along the angle  $\theta_2 = (1/2) \tan^{-1}(b_2/a_2)$ . Rotating into this coordinate frame then yields

$$A_4 = -\frac{15}{R_{\text{ein}}} (a_4 \cos 4\theta_2 + b_4 \sin 4\theta_2). \quad (29)$$

(The factor of  $-15$  comes from  $1 - k^2$ , which appears when we convert from Fourier coefficients in the potential to those in the density.) If  $A_4$  is negative (positive), the isodensity contours are boxy (disky). For B1422+231, our model with  $k_{\max} = 5$  has  $A_4 = -0.056$ . For comparison, the octopole amplitudes for the isophotes of real elliptical galaxies are in the range  $-0.015 \lesssim A_4 \lesssim 0.045$  (Bender et al. 1989; Saglia et al. 1993). In other words, the  $k_{\max} = 5$  model is much more boxy than real galaxies (which is not surprising in light of Figure 2(b)). If we increase  $k_{\max}$  to 9 (see below), we find  $A_4 = -0.021$  which is still rather boxy. Going to  $k_{\max} = 25$  yields  $A_4 = -0.010$ , which is no more boxy than many observed elliptical galaxies.



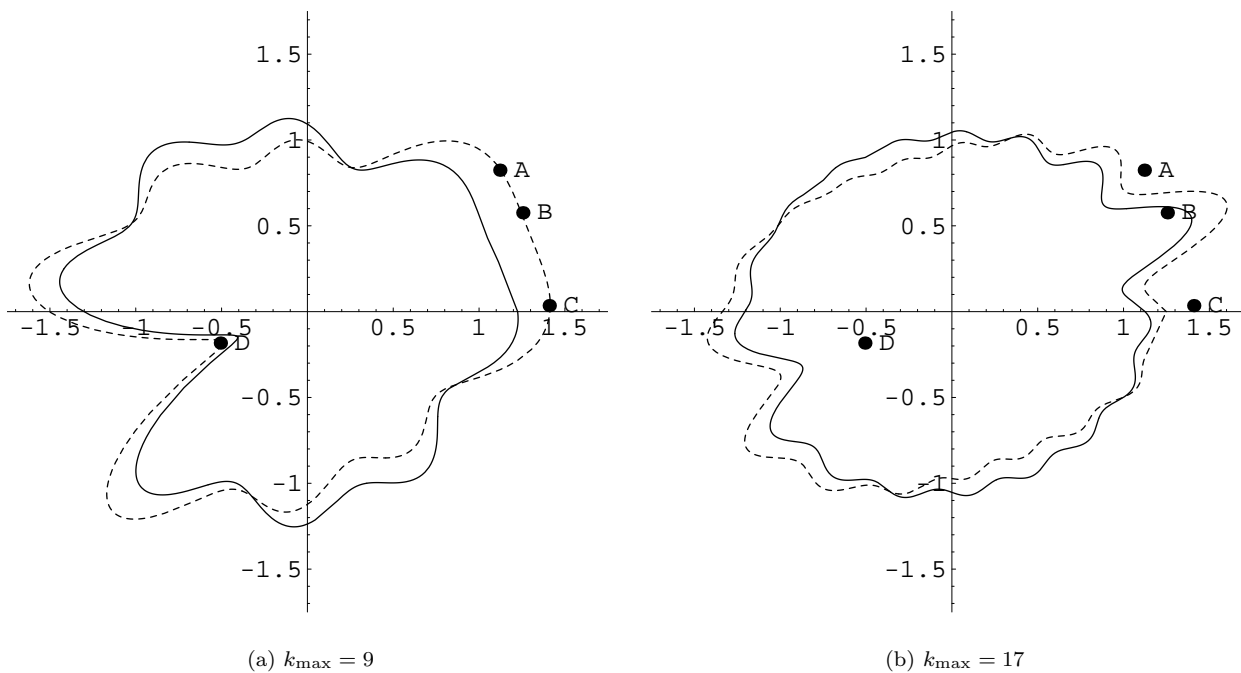
**Figure 2.** Isodensity contours with  $\kappa = 1/2$  (solid) and critical curves (dashed) for B1422+231. Panel (a) shows a model with  $k_{\max} = 5$  and no shear. Panel (b) shows the solution for the same value of  $k_{\max}$ , but nonzero shear parameters  $(\gamma_1, \gamma_2) = (0.029, 0.170)$ . The dots show the image positions (suppressed in panel (a) for clarity). Note that with nonzero shear, isodensity contours and critical curves are not identical.



**Figure 3.** Isodensity contours (solid) and critical curves (dashed) for minimum wiggle models of B1422+231. Panel (a) shows a model for  $k_{\max} = 9$  and shear parameters  $(\gamma_1, \gamma_2) = (0.028, 0.175)$ . Panel (b) shows a model for  $k_{\max} = 25$  and shear parameters  $(\gamma_1, \gamma_2) = (0.030, 0.167)$ .

**Table 1.** Fourier coefficients, normalized RMS wiggle, and shear parameters for the various multipole lens models discussed in this paper. We quote models that fit the data exactly.

System	B1422+231			B2045+265		B0712+472			B1933+503
$k_{\max}$	5	9	25	9	17	5	6	7	8
$R_{\text{Ein}}$	0.797	0.781	0.779	1.11	1.11	0.715	0.710	0.706	0.515
$a_2$	-0.0213	-0.0159	-0.0136	0.00158	-0.0211	-0.0306	-0.0424	-0.0361	-0.0112
$b_2$	-0.0689	-0.0492	-0.0517	0.0139	-0.0135	0.0394	0.0246	0.0239	-0.0586
$a_3$	-0.00817	-0.00359	-0.00223	-0.00928	-0.000950	-0.00333	0.000379	-0.0000154	0.00144
$b_3$	0.0132	0.000983	0.0000806	-0.0159	-0.00401	-0.00595	-0.000511	0.0000860	-0.00143
$a_4$	-0.00226	-0.00119	-0.000685	0.000673	0.000580	-0.00466	-0.000709	-0.000234	0.000869
$b_4$	0.00198	0.000195	-0.000196	0.00367	-0.000128	-0.000546	0.000113	0.000287	-0.000358
$\delta r_{\text{rms}}/R_{\text{Ein}}$	0.166	0.0528	0.0376	0.235	0.0943	0.215	0.0993	0.0546	0.126
$\gamma_1$	0.029	0.028	0.030	0.119	0.092	-0.044	-0.072	-0.066	-0.033
$\gamma_2$	0.170	0.175	0.167	0.125	0.090	-0.078	-0.092	-0.085	0.024

**Figure 4.** Isodensity contours (solid) and critical curves (dashed) for minimum wiggle models of B2045+265. Panel (a) shows the solution with  $k_{\max} = 9$  and  $(\gamma_1, \gamma_2) = (0.119, 0.125)$ . Panel (b) shows the solution with  $k_{\max} = 17$  and  $(\gamma_1, \gamma_2) = (0.092, 0.090)$ .

### 3.2 Higher Order Multipoles

Our next step is to include higher order multipole terms. In the case of B1422+231, the lowest order series for which a somewhat elliptical isodensity contour can be obtained is for  $k_{\max} = 9$  (see Figure 3(a)). As we increase  $k_{\max}$  the long-wavelength components of galactic structure disappear in favor of wiggles that are localized near the positions of the bright images A, B, and C (see Figure 3(b)). In other words, away from the images the model is smooth thanks to the minimum wiggle criterion. But there must be small-scale structure in the vicinity of the images in order to explain the observed flux ratios. Since the wiggles in the isodensity contour are not dramatic, it is not clear whether they should be interpreted as real features or just as approximations of other sorts of structure (such as CDM clumps).

Let us now turn our attention to B2045+265. We find

models that fit the data of Fassnacht et al. (1999) exactly. Unlike the case of B1422+231, the isodensity contour we obtain for  $k_{\max} = 9$  is completely unreasonable (see Figure 4(a)) and we must include multipoles of order 17 to obtain a remotely plausible model (see Figure 4(b)). Similar to B1422+231, we find that including higher order multipoles reduces the RMS wiggle, but pronounced deviations from ellipticity remain primarily near the bright images. This suggests that the structure required to fit the anomaly in B2045+265 truly is local to the images.

While the most obvious anomaly in B2045+265 is in the A/B/C triplet, it is worth noting that our models also have small-scale structure in the vicinity of the faint image D. Dobler & Keeton (2005) also concluded that the flux of image D is puzzling, and suggested that it has more to do with complex structure in the lens galaxy (such as an isophote twist) than with substructure per se. We cannot examine

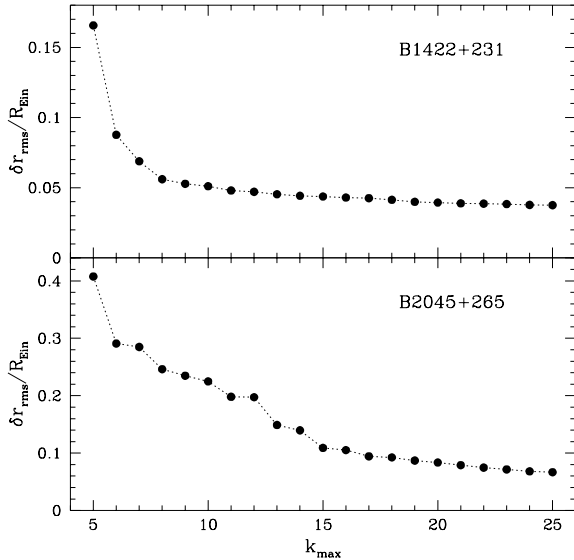


**Figure 5.** Normalized RMS wiggle ( $\delta r_{\text{rms}}/R_{\text{Ein}}$ ) as a function of  $k_{\text{max}}$ .

that hypothesis here because our models are intrinsically self-similar, but it will be interesting to keep this image in mind as we develop more general models in the future.

When examining isodensity contours, it may not be completely obvious that high-order models with small-scale undulations really have a smaller total wiggle than low-order models. To understand that, recall that our minimum wiggle criterion (see eq. 21) is designed to select the model whose isodensity contours deviate least from elliptical symmetry. As  $k_{\text{max}}$  increases, large-scale departures from ellipticity can be traded for smaller-scale features localized near the images in a way that does in fact decrease the total wiggle. Indeed, Figure 5 shows that  $\delta r_{\text{rms}}/R_{\text{Ein}}$  does decrease monotonically as the order of the multipole expansion increases. The decrease is rapid at small  $k_{\text{max}}$  but slows down as  $k_{\text{max}}$  increases, and that gives us a sense of the order at which the multipoles have basically converged to have the minimum amount of small-scale structure.

### 3.3 Measurement Uncertainties

So far we have considered models that fit the data exactly, since that is the natural outcome of an SVD analysis of the underconstrained matrix equation (18). However, it is important to consider whether measurement uncertainties affect our conclusions. While we could do this analysis for B2045+265, we believe that the puzzling flux of image D would complicate the interpretation. We turn instead to B0712+472.

We assume the image positions to be precise to within  $\pm 3$  mas, which is slightly conservative compared to the 1 mas uncertainties claimed by Jackson et al. (2000). For the flux ratios, we use the data of Koopmans et al. (2003), who found the uncertainties in the flux ratios of images B, C, and D relative to A to be 7.2%, 8.9%, and 43%, respectively. To be conservative, we construct models for which we take the

B/A and C/A uncertainties to be 10% and 20% (we always use the observed flux uncertainty of 43% for image D).

Since our formalism always produces models that fit the data exactly, the way we include measurement uncertainties is to add noise to the data and repeat our analysis. For every run, we perturb each data value by a random number drawn from a normal distribution with the appropriate dispersion, and then fit our model. We repeat this process 100 times, and select the case that has the smallest mean square wiggle. In this way we find the minimum wiggle model that fits the data within the measurement uncertainties.

Figure 6 shows the results for B0712+472. As we would expect, including measurement uncertainties produces models with slightly smaller wiggles. However, the changes are not significant enough to transform an implausible model into an acceptable solution.

### 3.4 A Multi-Source Lens Model

To conclude this section, we study B1933+503, where two sources are lensed by a single galaxy into two four-image configurations (Cohn et al. 2001, and references accompanying their Table 1). Both the image positions and flux ratios corresponding to one source are known, while only the image positions of the second source have been determined to reasonable precision. We therefore have  $N_c = 2(n_1 + n_2) + n_1 - 1 = 19$  constraints, compared with  $N_c = 3n - 1 = 11$  for the other systems we have analyzed, where  $n_1 = n_2 = 4$ . Since we must now fit a second source position, our list of parameters increases by two:  $N_p = 2k_{\text{max}} + 3$ . The matrix  $\mathbf{A}$  then has the dimensions  $[2(n_1 + n_2) + n_1 - 1] \times (2k_{\text{max}} + 3)$ , and is given by adding more rows that represent the additional position constraints, as follows:

$$\mathbf{A} = \begin{bmatrix} 1 & 0 & 0 & 0 & \alpha_{01}^{(1)} & \alpha_{21}^{(1)} & \beta_{21}^{(1)} & \cdots \\ \vdots & \vdots & \vdots & \vdots & \vdots & \vdots & \vdots & \vdots \\ 1 & 0 & 0 & 0 & \alpha_{0n_1}^{(1)} & \alpha_{2n_1}^{(1)} & \beta_{2n_1}^{(1)} & \cdots \\ 0 & 1 & 0 & 0 & \hat{\alpha}_{01}^{(1)} & \hat{\alpha}_{21}^{(1)} & \hat{\beta}_{21}^{(1)} & \cdots \\ \vdots & \vdots & \vdots & \vdots & \vdots & \vdots & \vdots & \vdots \\ 0 & 0 & 1 & 0 & \alpha_{01}^{(2)} & \alpha_{21}^{(2)} & \beta_{21}^{(2)} & \cdots \\ \vdots & \vdots & \vdots & \vdots & \vdots & \vdots & \vdots & \vdots \\ 0 & 0 & 1 & 0 & \alpha_{0n_2}^{(2)} & \alpha_{2n_2}^{(2)} & \beta_{2n_2}^{(2)} & \cdots \\ 0 & 0 & 0 & 1 & \hat{\alpha}_{01}^{(2)} & \hat{\alpha}_{21}^{(2)} & \hat{\beta}_{21}^{(2)} & \cdots \\ \vdots & \vdots & \vdots & \vdots & \vdots & \vdots & \vdots & \vdots \\ 0 & 0 & 0 & 0 & \gamma_{01}^{(1)} & \gamma_{21}^{(1)} & \delta_{21}^{(1)} & \cdots \\ \vdots & \vdots & \vdots & \vdots & \vdots & \vdots & \vdots & \vdots \\ 0 & 0 & 0 & 0 & \gamma_{0,n_1-1}^{(1)} & \gamma_{2,n_1-1}^{(1)} & \delta_{2,n_1-1}^{(1)} & \cdots \end{bmatrix} \quad (30)$$

We first consider just the primary set of four images, which are labeled 1, 3, 4, and 6. (There is a flux ratio anomaly such that image 4 is brighter than expected.) The minimum wiggle model with  $k_{\text{max}} = 8$  that fits these images is not very plausible — it has a large protrusion near image 4, and a smaller one near image 1 — but at least the

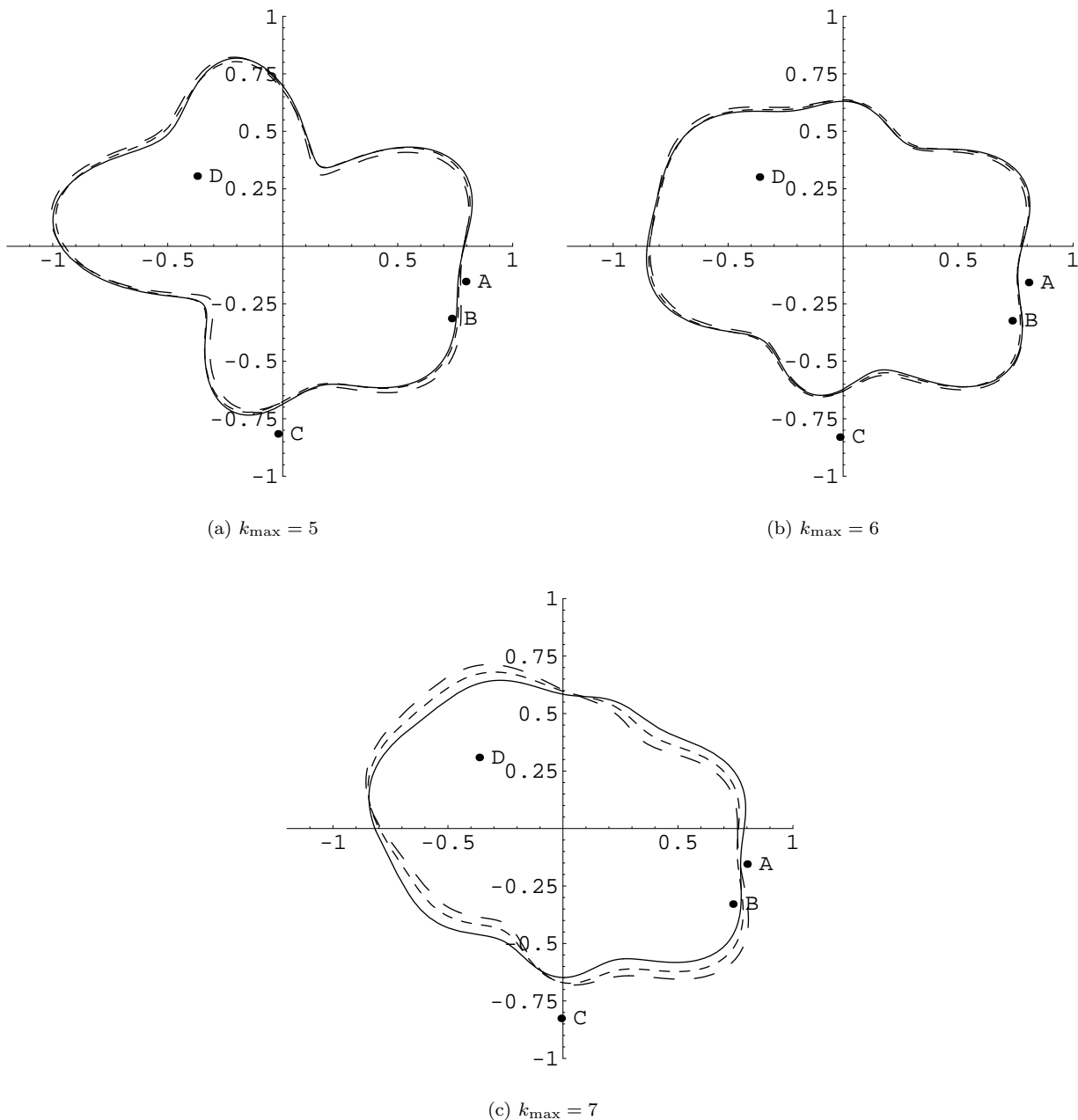


**Figure 6.** Model isodensity contours for B0712+472 with increasing multipole order. The solid curve in each panel fits the data exactly. The short and long-dashed curves fit the data to within 10% and 20% flux uncertainties, respectively (except for faint image D, whose flux uncertainty is fixed at the observed value of 43%; see Koopmans et al. 2003).

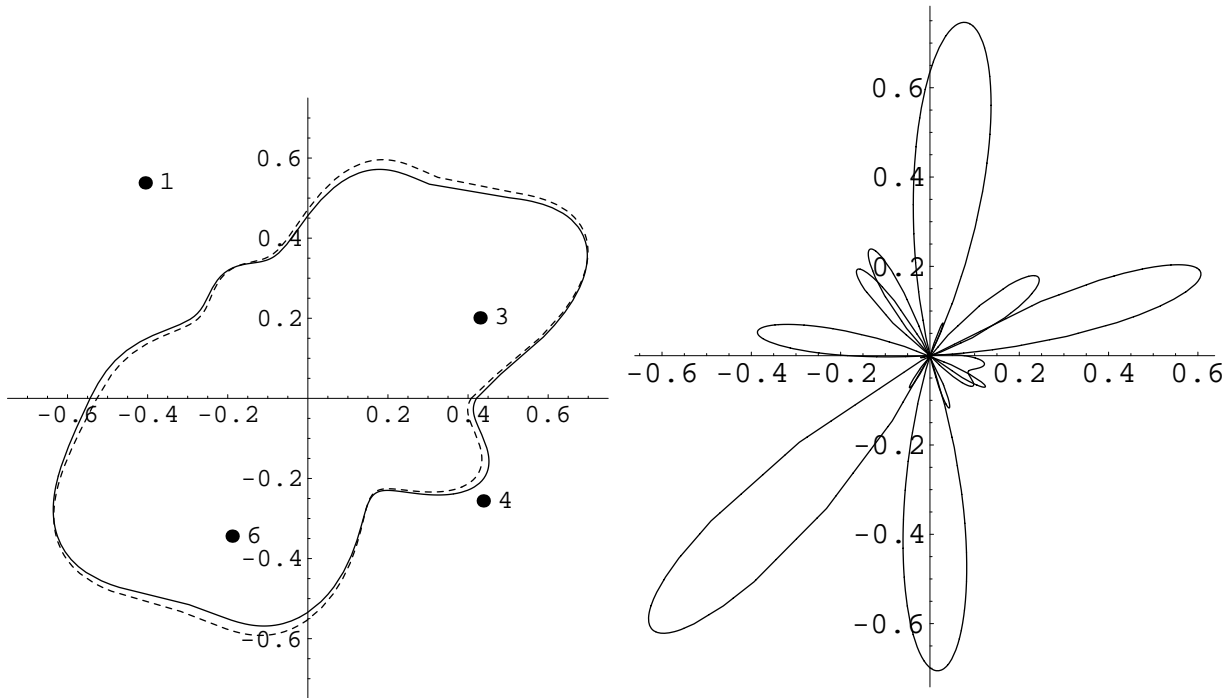
density is positive definite. When we add the additional constraints from the positions of images 2a, 2b, 5, and 7, they dramatically reduce the solution space ( $k_{\max} = 8$  is the lowest order case that is not over-constrained). The only models that remain are unphysical. Modestly increasing  $k_{\max}$  does not help. In other words, multipole models cannot simultaneously fit the anomalous fluxes of images 1, 3, 4 and 6, and the positions of images 2a, 2b, 5 and 7.

#### 4 CONCLUSIONS

We have shown that extending the method of Evans & Witt (2003) by including external shear and higher-order Fourier terms is essential for understanding whether multipole models can fit observed lenses. The results for B1422+231 we have obtained are of a very different character from those of Evans & Witt (2003). Even so, we cannot conclude that the multipole approach provides an acceptable explanation of flux ratio anomalies.

The system B2045+265 requires multipoles of order





(a) Including image positions and flux ratios for images 1, 3, 4, and 6 only

(b) Including all constraints

**Figure 7.** Isodensity contours (solid) and critical curves (dashed) for two models of B1933+503. Panel (a) includes the constraints for images 1, 3, 4 and 6. Panel (b) shows a model in which all of the observational constraints have been fit. Both models account for external shear and multipoles up to  $k_{\max} = 8$ .

$\gtrsim 15$ . Even this level of small-scale structure leads to a rather wiggly angular dependence of density near the three bright images. Next, our analysis of B1933+503 reveals that a fundamental difficulty exists in fitting a multi-source lens with a simple multipole model. Finally, our method naturally finds models that fit the data exactly, but we have shown that our conclusions are not very sensitive to measurement uncertainties.

Our results suggest that there is a more fundamental problem with the global approach taken by Evans & Witt (2003) and ourselves in the current paper. It is possible that the problem simply comes from our choice of small scale structure. Sines and cosines provide a useful but by no means unique basis for carrying out a series expansion of the angular part of the potential. In addition, we have assumed a particular form for the radial dependence — notably self-similarity — which may need to be modified in order to find an acceptable galactic density function. While the present analysis seems to rule out simple multipole models, the question of whether CDM clumps provide the only plausible solution has yet to be fully answered.

## ACKNOWLEDGEMENTS

We thank Arthur Kosowsky, Tad Pryor, and Jerry Sellwood for helpful discussions. ABC is supported by an NSF Graduate Research Fellowship.

## REFERENCES

- Bender R., Surma P., Döbereiner S., Möllenhoff C., Madejsky R., 1989, *A&A*, 217, 35  
 CASTLES Website, <http://cfa-www.harvard.edu/castles/>  
 Cohn J. D., Kochanek C. S., McLeod B. A., Keeton C. R. 2001, *ApJ*, 554, 1216  
 Dalal N., Kochanek C. S., 2002, *ApJ*, 572, 25  
 Dobler G., Keeton C. R., 2005, *astro-ph/0502436*  
 Evans N. W., Witt H. J., 2001, *MNRAS*, 327, 1260  
 Evans N. W., Witt H. J., 2003, *MNRAS*, 345, 1351  
 Falco E. E., Lehár J., Perley R. A., Wambsganss J., Gorenstein M. V., 1996, *AJ*, 112, 897  
 Fassnacht C. D., et al., 1999, *AJ*, 117, 658  
 Gaudi B. S., Petters A. O., 2002, *ApJ*, 574, 970  
 Impey C. D., Foltz C. B., Petry C. E., Browne I. W. A., Patnaik A. R., 1996 *ApJ*, 307, L53  
 Jackson N., Xanthopoulos E., Browne I. W. A., 2000, *MNRAS*, 311, 389  
 Keeton C. R., Gaudi B. S., Petters A. O., 2003, *ApJ*, 598, 138  
 Keeton C. R., Gaudi B. S., Petters A. O., 2005, *astro-ph/0503452*  
 Keeton C. R., Kochanek C. S., Falco E. E., 1998, *ApJ*, 509, 561  
 Keeton C. R., Kochanek C. S., Seljak U., 1997, *ApJ*, 482, 604  
 Klypin A., Kravtsov A. V., Valenzuela O., Prada F., 1999,

- ApJ, 522, 82  
Kochanek C. S., 1991, ApJ, 373, 354  
Kochanek C. S., Dalal N., 2004, ApJ, 610, 69  
Kochanek C. S., Schneider P., Wambsganss J., 2004, Part 2 of Gravitational Lensing: Strong, Weak & Micro, Proceedings of the 33rd Saas-Fee Advanced Course, G. Meylan, P. Jetzer & P. North, eds. (Springer-Verlag: Berlin)  
Koopmans L. V. E., Biggs A., Blandford R. D., Browne I. W. A., Jackson N. J., Mao S., Wilkinson P. N., de Bruyn A. G., Wambsganss J., 2003, ApJ, 595, 712  
Kundić T., Hogg D. W., Blandford R. D., Cohen J. G., Lubin L. M., Larkin J. E., 1997, AJ, 144, 2276  
Mao S., Schneider P., 1998, MNRAS, 295, 587  
Metcalf R. B., Madau P., 2001, ApJ, 563, 9  
Momcheva I., Williams K., Keeton C. R., Zabludoff A., 2005, ApJ submitted  
Moore B., Ghigna S., Governato F., Lake G., Quinn T., Stadel J., Tozzi P., 1999, ApJ, 524, L19  
Patnaik A. R., Kembell A. J., Porcas R. W., Garrett M. A., 1999, MNRAS, 307, L1  
Saglia R. P., Bender R., Dressler A., 1993, A&A, 279, 75  
Schneider P., Weiss A., 1992, A&A, 260, 1  
Witt H. J., Mao S., Keeton C. R., 2000, ApJ, 544, 98  
Zhao H., Pronk D., 2001, MNRAS, 320, 401